

# CT10 parton distributions and other developments in the global QCD analysis

Marco Guzzi<sup>1</sup>, Pavel Nadolsky<sup>1</sup>,  
Edmond Berger<sup>2</sup>, Hung-Liang Lai<sup>3</sup>, Fredrick Olness<sup>1</sup>, and C.-P. Yuan<sup>4</sup>

<sup>1</sup> Department of Physics, Southern Methodist University, Dallas, TX 75275 USA

<sup>2</sup> High Energy Physics Division, Argonne National Laboratory, Argonne, Illinois 60439, USA

<sup>3</sup> Taipei Municipal University of Education, Taipei, Taiwan

<sup>4</sup> Dept. of Physics & Astronomy, Michigan State University, E. Lansing, MI 48824, USA

We summarize several projects carried out by the CTEQ global analysis of parton distribution functions (PDFs) of the proton during 2010. We discuss a recently released CT10 family of PDFs with a fixed and variable QCD coupling strength; implementation of combined HERA and Tevatron lepton asymmetry data sets; theoretical issues associated with the analysis of  $W$  charge asymmetry in PDF fits; PDFs for leading-order shower programs; and constraints on new color-octet fermions from the hadronic data.

November 10, 2018

## Contents

CTEQ PDFs in 2010 . . . . .	2
Implementation of new data sets . . . . .	2
Constraints from combined DIS data by HERA-1 . . . . .	2
Agreement with the HERA data at small and large $x$ . . . . .	3
Tevatron Run-2 $W$ lepton asymmetry data . . . . .	4
CT10 predictions for collider observables . . . . .	9
New PDF parametrizations; advancements in statistical analysis . . . . .	9
Dijet invariant mass distributions . . . . .	9
Uncertainty due to $\alpha_s$ in CTEQ6.6 and CT10 PDF analyses . . . . .	12
Constraints on new physics from a global PDF analysis . . . . .	13
PDFs for leading-order showering programs . . . . .	15
References . . . . .	16

## CTEQ PDFs in 2010

Parton distribution functions (PDFs) are essential nonperturbative functions of quantum chromodynamics (QCD). They describe the internal structure of the proton in high-energy scattering at the Fermilab Tevatron collider, CERN Large Hadron Collider, and in other experiments. Modern PDFs continuously evolve to include emerging theoretical developments and latest data from hadronic experiments, and to provide reliable estimates of uncertainties associated with various experimental and theoretical inputs. In this paper, we review the recent progress in the determination of the PDFs by CTEQ collaboration [1, 2, 3, 4], which is one of three groups involved in the global analysis of hadronic data, besides the MSTW [5] and NNPDF [6] groups.

### Implementation of new data sets

Since the release of the previous general-purpose CTEQ6.6 PDF set [7] in 2008, new data sets have been published in every category of processes included in the global QCD analysis: deep inelastic scattering (DIS), vector boson production, and inclusive jet production. These data sets include a combination of DIS cross sections by the H1 and ZEUS collaborations in HERA-1 [8], as well as measurements of  $W$  lepton asymmetry [9, 10, 11],  $Z$  rapidity distributions [12, 13], and single-inclusive jet cross sections [14, 15] by CDF and DØ collaborations at the Tevatron. All these new data are included in our latest global analysis, designated as CT10 [3].

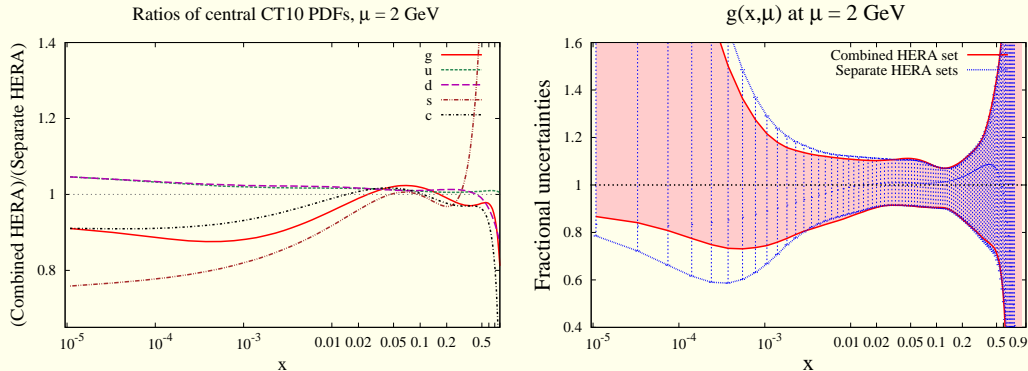
The new analysis produced two families of general-purpose PDF sets, denoted as CT10 and CT10W, which differ in their treatment of the Tevatron  $W$  lepton asymmetry data sets affecting the ratio of  $d$  and  $u$  quark PDFs at  $x > 0.1$ , as discussed below, but are very similar in all other aspects. In addition, we examined the dependence of the PDFs on the QCD coupling  $\alpha_s(M_Z)$  and provided special CT10AS PDF sets with a varied  $\alpha_s(M_Z)$  in the range 0.113-0.123 to evaluate the combined PDF- $\alpha_s$  uncertainty in practical applications. The CT10 PDFs are obtained at next-to-leading order in  $\alpha_s$ , using the general-mass treatment of charm and bottom quark contributions to hadronic observables. To support calculations for heavy-quark production in the fixed-flavor-number factorization scheme, we also provide additional PDF sets CT10(W).3F and CT10(W).4F, obtained from the best-fit CT10.00 and CT10W PDF sets by QCD evolution with three and four active quark flavors. All the PDF sets discussed in this paper (CT10, CT10W, CT10AS, CT10XF, and CT09MC) are available as a part of the LHAPDF library [16] and from our website [17].

### Constraints from combined DIS data by HERA-1

The CT10/CT10W fits include a combined set of HERA-1 cross sections on neutral-current and charged-current DIS [8], which replaces 11 separate HERA-1 data sets used in CTEQ6.6 and earlier fits. In the combined set, systematic factors that are in common to both experiments were presented as a table of 114 correlated systematic errors, whose effect is shared by each data point in all scattering channels. As a result of the cross calibration of detection parameters between the H1 and ZEUS experiments, the combined data set has a reduced total systematic uncertainty. Consequently, the PDF uncertainties at  $x < 10^{-3}$ , in the region where the HERA data provide tightest constraints on the gluon and heavy-quark PDFs, are also reduced.

The impact of the combined HERA-1 set on the PDFs is illustrated by Fig. 1, showing relative differences between the CT10 PDF set, fitted to the combined HERA-1 data, and a counterpart fit, fitted to the separate HERA-1 data sets. In the left subfigure, comparing the best-fit PDFs in the two fits, one observes reduction in the gluon and charm PDFs at  $x < 0.05$ , accompanied by a few-percent increase in the  $u$  and  $d$  quark PDFs in the same  $x$  region. The strange quark PDF shows a larger suppression (up to 25% at  $x = 10^{-5}$ ), which, however, is small compared to the large

Figure 1: Left: ratios of CT10 central PDFs fitted to the combined HERA-1 data set and to the separate HERA-1 data sets, at scale  $\mu = 2$  GeV. Right: bands of the PDF uncertainty (relative to the the central PDF set) for the gluon PDF in (red) CT10 with the combined HERA-1 data, (blue) CT10 with the separate HERA data.  $g(x)$ ,  $Q = 2$  GeV.



PDF uncertainty associated with this flavor. Fig. 1 (right) shows the asymmetric fractional PDF uncertainty, computed as in [18], and normalized to the best-fit gluon PDF of each fit. The impact of the HERA-1 data on the uncertainties of the gluon and charm PDFs is visible in the small- $x$  region, starting from  $x = 10^{-3}$  and going down to  $x = 10^{-5}$ , where the error bands contract upon the combination of the HERA data sets. In the large  $x$  region, the error bands for the combined and separate HERA data sets are almost coincident.

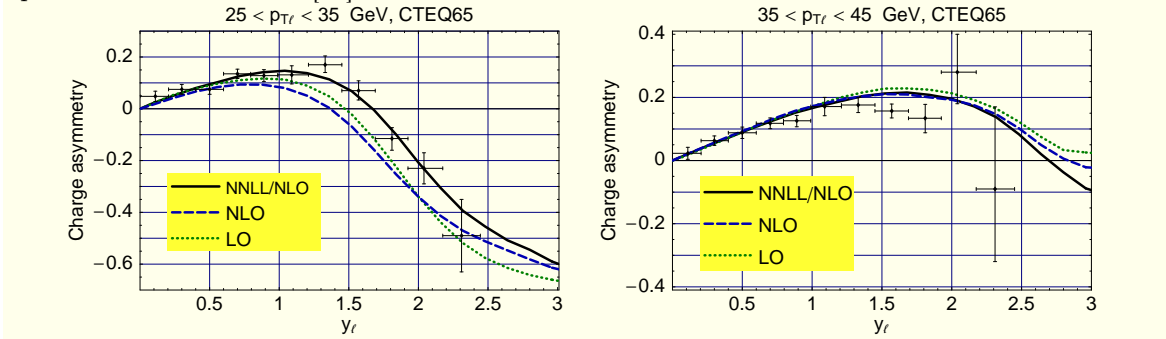
### Agreement with the HERA data at small and large $x$

The overall agreement of the CT10 fit with the combined HERA-1 data is slightly worse than with the separate HERA-1 data sets, as a consequence of some increase in  $\chi^2/\text{d.o.f.}$  for the neutral-current DIS data at  $x < 0.001$  and  $x > 0.1$ . While the origin of this increase is uncertain, the pattern of point-to-point contributions to  $\chi^2$  from the data is consistent with random fluctuations that turn out to be larger than normally expected. No systematic discrepancies between the HERA-1 DIS data and theoretical cross sections are observed, suggesting that the NLO QCD theory based on CT10 PDFs is generally consistent with the HERA experiments in the region  $Q > 2$  GeV included in the CT10 fit.

In looking for potential systematic deviations of this kind, we examined the agreement with the data as a function of either  $x$  and  $Q$ , or the “geometric scaling” variable  $A_{gs} = Q^2 x^{0.3}$  proposed by NNPDF authors in Refs. [19, 20]. At  $A_{gs} \rightarrow 0$ , DGLAP factorization that is required to introduce the PDFs can be invalidated by higher-twist terms or saturation; the question is whether such effects may bias the determination of the PDFs at  $A_{gs} \gtrsim 0.1$ , in the kinematical region commonly included in the global fits.

Indeed, the NNPDF study finds that the PDFs fitted to the HERA data above some cutoff value ( $A_{gs} > A_{cut}$ ), disagree at the  $2\sigma$  level with the HERA data in the “causally connected” region below the cutoff,  $0.5 < A_{gs} < A_{cut}$ . The NNPDF analysis is realized in the zero-mass approximation and includes DIS data in the less safe region  $\sqrt{2}$  GeV  $< Q < 2$  GeV. We repeated the  $A_{cut}$  fits proposed by NNPDF as closely as possible, in the general-mass factorization scheme, and in the region of  $Q > 2$  GeV where our data are customarily selected to suppress higher-order

Figure 2: Comparison of CDF Run-2 lepton asymmetry data [9] with LO, NLO, and resummed predictions from ResBos [35].



and higher-twist terms. While the outcomes of our  $A_{cut}$  fits bear some similarity to those by NNPDF, the discrepancies between our best-fit NLO predictions and the data below  $A_{cut}$  are less significant than those quoted by NNPDF and are characterized by a large PDF uncertainty. Thus, our fits do not corroborate the existence of stable deviations of the NLO DGLAP factorization from the data, if the lower  $Q$  bound is chosen to be above 2 GeV. See further discussion in the appendix of Ref. [3].

### Tevatron Run-2 $W$ lepton asymmetry data

**The puzzle of Run-2  $W$  asymmetry.** Recently, the Fermilab D $\bar{O}$  Collaboration [10, 11] published measurements of  $W$  charge asymmetry  $A_\ell(y_\ell)$  in electron ( $\ell = e$ ) and muon ( $\ell = \mu$ ) decay channels, presented as a function of the rapidity of the charged decay lepton. NLO predictions based on CTEQ6.1 and CTEQ6.6 sets disagree with these data at surprisingly large  $\chi^2/N_{pt}$  of about 5. The values of  $\chi^2/N_{pt}$  can be even higher (as high as 20) for some other recent (N)NLO PDF sets [11, 22]. Such level of disagreement may appear surprising, given that the Tevatron  $W$  asymmetry probes the ratio of  $d$  and  $u$  quark PDFs [21] in the region  $x > 0.1$ , where they are known quite well from the other experiments.

**Sensitivity to the  $d/u$  slope.** The discrepancy involving  $A_\ell$  can be understood in part by noticing that the  $A_\ell$  measurement is very sensitive to the average  $x$  derivative (slope) of the ratio of the up and down quark PDFs,  $d(x, M_W)/u(x, M_W)$ , computed between the typical  $x$  values  $x_{1,2} = M_W e^{\pm y_W}/\sqrt{s}$  accessible at a given boson rapidity  $y_W$  [21, 23]. Small variations of the  $d/u$  slopes in distinct PDF sets can change the behavior of  $A_\ell$  by large amounts [24].

**Impact of soft gluon resummation.** Another factor at play are soft parton emissions with small transverse momenta, which affect the precise  $A_\ell$  data because of constraints imposed on the transverse momentum  $p_{T\ell}$  of the decay charged lepton. The  $A_\ell$  data require  $p_{T\ell}$  to be above 20-25 GeV in order to suppress charged leptons from background processes that do not involve a  $W$  boson decay. In addition, the Run-2  $A_\ell$  data are organized into bins of  $p_{T\ell}$ , *e.g.*, 25-35 GeV and 35-45 GeV in order to better probe the  $x$  dependence of  $d(x, Q)/u(x, Q)$  [9]. While such binning amplifies the sensitivity of the  $A_\ell$  data to the PDFs, it also makes it dependent on the shape of the  $p_{T\ell}$  distribution near the Jacobian peak at  $p_{T\ell} \approx M_W/2 \approx 40$  GeV or, equivalently, to the transverse momentum ( $Q_T$ ) distribution of  $W$  bosons at  $Q_T < 20$  GeV, where large logarithms  $\ln(Q_T/Q)$  dominate the cross section. A calculation that evaluates these logarithms to all orders in  $\alpha_s$  [25, 26, 27], in addition to including the leading NNLO corrections [29, 28], results in somewhat different

Figure 3: Comparison of the CT10W and CTEQ6.6 predictions with the DØ Run-II data for the electron charge asymmetry  $A_e(y_e)$  for an integrated luminosity of  $0.75 \text{ fb}^{-1}$  [10]

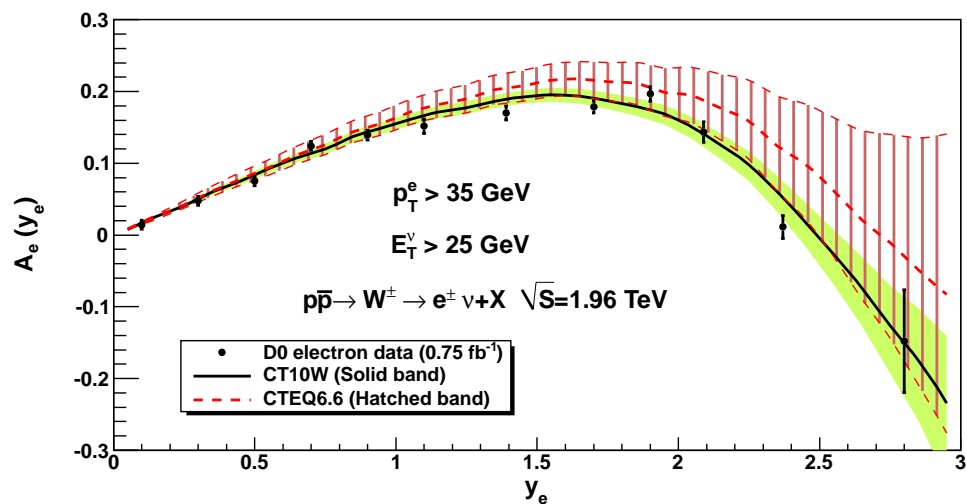
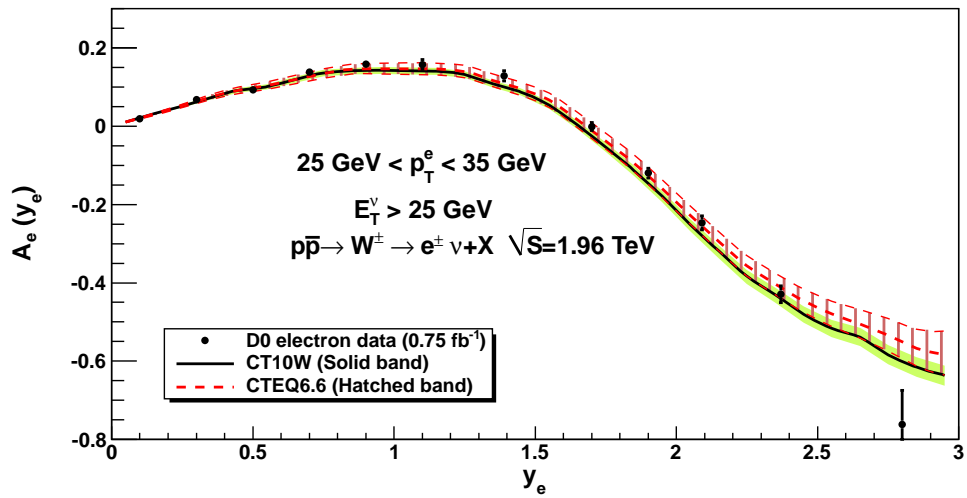
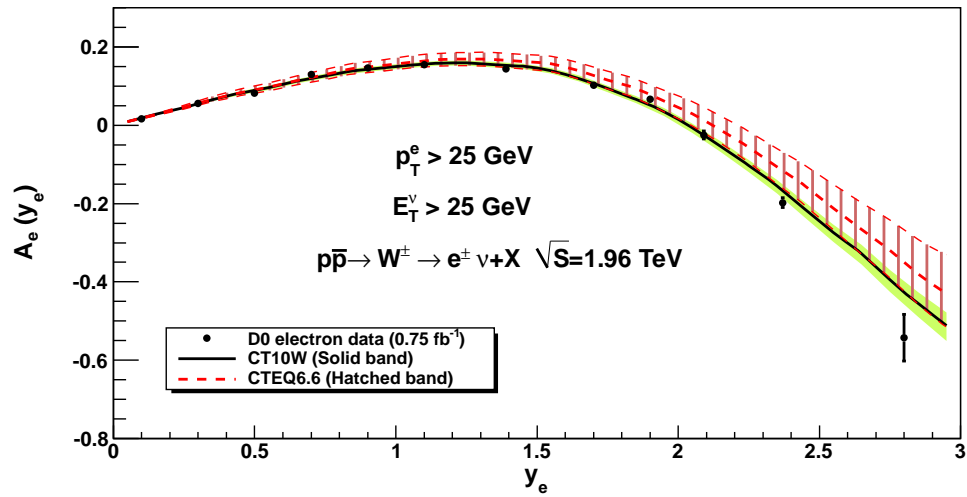
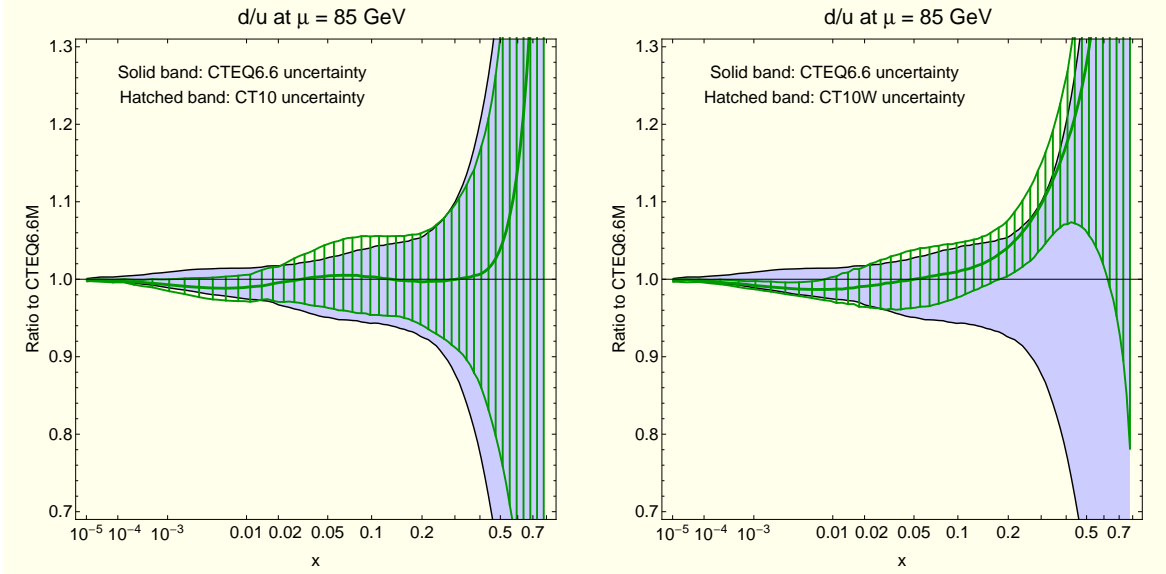


Figure 4: The  $d/u$  ratio for CT10 (left) and CT10W (right) versus that for CTEQ6.6, at scale  $\mu = 85$  GeV.



predictions for  $A_\ell$  than (N)NLO calculations without resummation, like those implemented in the other available codes [30, 32, 33, 34].

In CT10 fits, the QCD radiative contributions to  $A_\ell(y_\ell)$  are implemented to the next-to-next-to-leading accuracy in  $Q_T$  logarithms and NLO accuracy in the QCD coupling strength using the program ResBos that realizes the approach of Refs. [25, 26, 27]. The resummed differential distributions for  $d\sigma/dQ_T$  and  $d\sigma/dp_{T\ell}$  both agree well with the data, in contrast to the fixed-order results. We thus expect that the resummed predictions for  $A_\ell$  implemented in the CT10 fit are more reliable as well.

The magnitude of differences between the NLO and resummed predictions is illustrated by Fig. 2, comparing the CDF Run-2  $A_\ell(y_\ell)$  data [9] with LO, NLO, and resummed NNLL-NLO predictions from ResBos. The NLO and resummed curves are clearly distinct in the bin  $25 < p_{T\ell} < 35$  GeV, shown in the left panel, and some differences are also seen in the bin  $35 < p_{T\ell} < 45$  GeV, shown in the right panel. The shape of the NLO prediction in this comparison is not unique and depends on the phase space slicing parameter  $Q_T^{sep}$  that defines the size of the lowest  $Q_T$  bin where the real and virtual NLO singularities are canceled [26]. In the current comparison,  $Q_T^{sep} = 3\text{GeV}$ , but other values of  $Q_T^{sep}$  are equally possible and would lead to NLO predictions lying closer to, or further from, the shown resummed curve. Such variations due to  $Q_T^{sep}$  or factorization scale indicate that resummation effects are important and should be included in precise fits to  $A_\ell$ .<sup>1</sup>

**Numerical predictions of the CT10W analysis.** When included in the CTEQ global analysis, the CDF measurements of  $A_\ell$  in Tevatron Run-1 [37] and Run-2 [9] agree well with the other data sets constraining the  $d/u$  ratio, provided by deep inelastic scattering on proton and

<sup>1</sup>The NNLO contributions produce marginal modifications compared to the NNLL-NLO result included in the CT10 analysis. We examined these contributions by redoing the calculation for  $A_\ell(y_\ell)$  after adding the exact  $\alpha_s^2$  correction for  $W$  bosons produced with non-zero transverse momentum, which captures a large part of the full NNLO effect. The changes were found to be small and inconsequential in the current fit.

deuteron targets by the NMC [38] and BCDMS [39, 40] collaborations. However, the most precise Run-2 lepton  $A_\ell$  data by the DØ Collaboration [10, 11] run into disagreement with the NMC and BCDMS deuteron DIS data, and in addition, exhibit some tension among themselves. Because of these disagreements, two separate fits are produced: CT10, which does not contain the DØ  $W$  electron asymmetry sets, and CT10W, in which they are included using weight factors larger than 1 to ensure an acceptable fit. We obtain  $\chi^2/N_{pt} = 91/45 = 2$  in the CT10W fit to the Run-2  $A_\ell$ , which is a significant improvement compared to  $200/45 = 4.4$  obtained in CT10. Comparison of NNLL-NLO predictions based on CT10W PDFs with the electron charge asymmetry data is presented in Fig. 3.

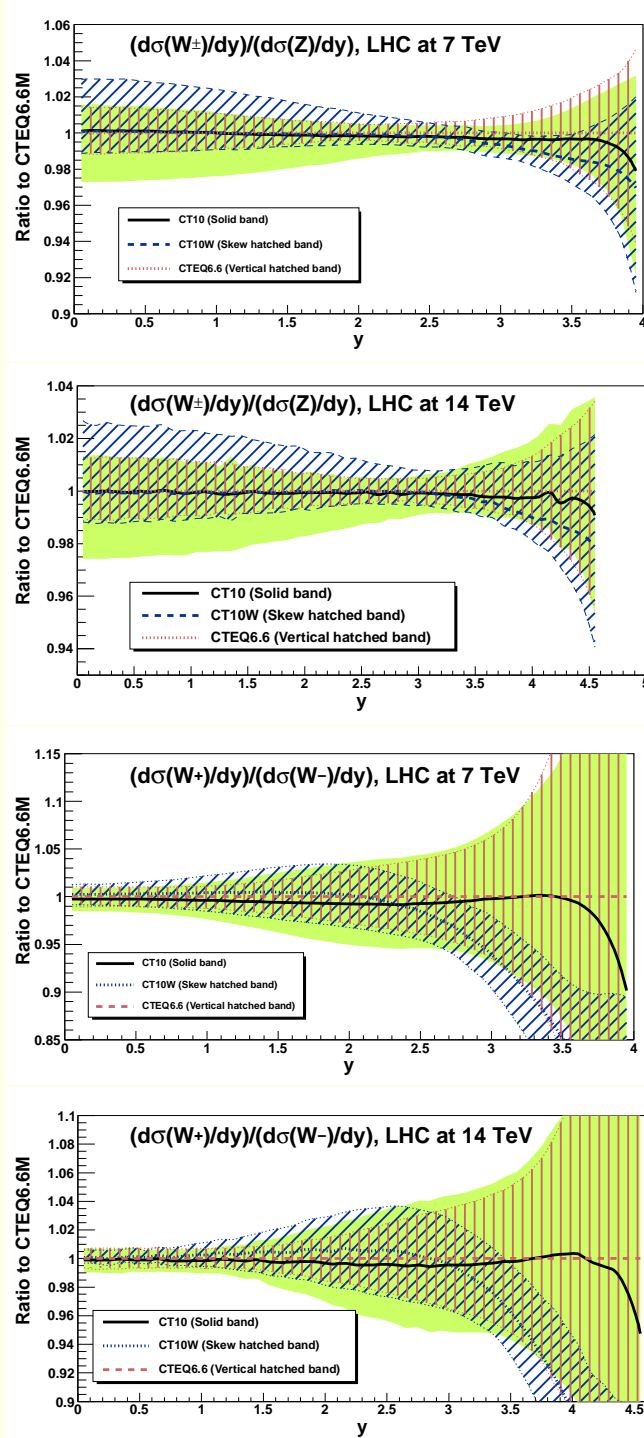
In the CT10W analysis, the inclusion of the Run-2  $A_\ell$  data increases the slope of  $d(x)/u(x)$  at  $x$  between 0.1 and 0.5 and reduces its uncertainty, as compared to CTEQ6.6 and CT10. This is illustrated by Fig. 4, which shows uncertainty bands for the  $d/u$  ratio in CTEQ6.6, CT10, CT10W PDFs vs. the momentum fraction  $x$  at scale  $Q = 85$  GeV .

Fig. 5 shows the ratios  $r_{WZ} = \sigma(pp \rightarrow W^\pm X)/\sigma(pp \rightarrow Z^0 X)$  and  $r_{W^+W^-} = \sigma(pp \rightarrow W^+ X)/\sigma(pp \rightarrow W^- X)$  of the rapidity distributions in  $W^\pm$  and  $Z$  boson production at the LHC, obtained using CTEQ6.6, CT10 and CT10W PDFs and divided by the predictions based on the CTEQ6.6M set. Here, the reduction of the uncertainty bands in the ratio of  $W^+$  to  $W^-$  cross sections predicted based on the CT10W PDFs, as compared to CT10, is again evident.

**Comparison with other fits.** The MSTW'08 [5] and NNPDF2.0 [36] groups have also explored the impact of the DØ Run-2  $A_\ell$  data. While their conclusions are broadly compatible with ours, the details vary. For example, in the CT10W fit, we find that all three  $p_{T\ell}$  bins of the electron  $A_\ell$  data and the second  $p_{T\ell}$  bin of the fit can be combined with the other data sets, despite the remaining disagreement with the deuteron DIS experiments. NNPDF, on the other hand, finds that all bins of the muon  $A_\ell$  are compatible with the deuteron DIS and all other experiments, but incompatible with the second and third  $p_{T\ell}$  bins of the electron  $A_\ell$ . NNPDF compute their NLO  $A_\ell$  predictions using the DYNLO code [34], which can deviate from the resummed NNLL+NLO predictions by ResBos used by CTEQ, as discussed above.

The resolution of the Run-2  $A_\ell$  puzzle thus seems to require consistent implementation of perturbative QCD calculations both in experimental analyses and PDF fits, including small- $Q_T$  resummed contributions, when constraints on the lepton  $p_{T\ell}$  are imposed. For greater precision it may be preferable to perform the small- $Q_T$  resummation for every component of the angular distribution of the decay lepton [41], in addition to the resummation for two dominant angular components that is currently implemented in ResBos. Resummation of the full dependence on the polar and azimuthal angles  $\theta$  and  $\phi$  of the lepton in the vector boson rest frame may be important especially in situations in which the experimental coverage is not uniform in all directions, or when there are gaps in the coverage. Normally the angular coverage varies with rapidity, notably at large rapidity, and this variation may well affect the lepton asymmetry, with different consequences in different experiments.

Figure 5: CT10, CT10W, and CTEQ6.6 PDF uncertainty bands for the ratios  $(d\sigma(W^\pm)/dy)/(d\sigma(Z)/dy)$  (upper two subfigures) and  $(d\sigma(W^+)/dy)/(d\sigma(W^-)/dy)$  (lower two subfigures), at the LHC energies 7 and 14 TeV.



## CT10 predictions for collider observables

Fig. 6 compares the NLO total cross sections, obtained using CT10 and CT10W PDFs, to those obtained using CTEQ6.6 PDFs, for some selected processes at the Tevatron Run-2 and the LHC at  $\sqrt{s} = 7$  TeV. For most of the cross sections, CT10 and CT10W sets provide similar predictions and uncertainties, which are also in good agreement with those from CTEQ6.6 (*i.e.*, well within the PDF uncertainty band). At the LHC, the PDF uncertainties in CT10 and CT10W predictions for some processes are larger than those in the counterpart CTEQ6.6 predictions, reflecting the changes in the framework of the fit discussed in the next paragraph. At the Tevatron, the CT10(W) PDF uncertainties tend to be about the same as those for CTEQ6.6, with a notable exception of  $t\bar{t}$  production cross sections, which have a smaller PDF uncertainty with the CT10W set, because of stricter constraints on the up- and down-quark PDFs at the relevant  $x$  values.

## New PDF parametrizations; advancements in statistical analysis

The CT10 global analysis implements several new features which were not available in the previous studies. The systematic uncertainty associated with the overall normalization factor in each of the data sets is handled in the same manner that all other systematic error parameters are handled. The best-fit values of the normalizations are found algebraically, and their variations are included in the final estimate of the PDF uncertainties. More flexible parametrizations are assumed for the gluon,  $d$ -quark, and strange quark PDFs at the initial scale 1.3 GeV, to reduce biases in predictions in kinematical regions where the constraints from the data are weak. Finally, a new statistical procedure is introduced to guarantee the agreement of the fits at 90% C.L. with all included experiments, for any PDF eigenvector set produced by the error analysis. This is realized by adding an extra contribution to the total  $\chi^2$ , which guarantees the quality of fit to each individual data set and halts the displacement along any eigenvector early, if necessary, to prevent one or more individual data sets from being badly described. The old procedure to enforce the 90% C.L. agreement with all experiments in the CTEQ6 family of fits, by artificially increasing statistical weights of  $\chi^2$  contributions from those experiments that may be fitted poorly by some PDF eigenvector sets, is phased out by this more efficient method. As a result of these changes, the CT10/CT10W PDF uncertainty may be smaller or larger than the CTEQ6.6 uncertainty, depending on whether the improved constraints from the data outweigh the increased uncertainty due to the relaxed PDF parametrizations and variations of normalizations during the determination of PDF eigenvector sets.

## Dijet invariant mass distributions

Fig.7 compares NLO predictions based on CTEQ6.6, CT10, and CT10W PDFs with the data on the dijet invariant mass distribution  $d\sigma/dM_{jj}$  reported recently by the DØ Collaboration [42]. These data are not included in the CT10 fit, but they are sensitive to the same scattering subprocesses, and include the same events, as the single-inclusive jet data constraining the gluon PDF in the CT10 fit. The cross sections are normalized to the theory prediction based on the central CT10 PDF set. The statistical and systematic errors of the DØ data are added in quadrature. The renormalization and factorization scales in the theoretical predictions are set equal to a half of the average  $p_T$  of the jets,  $\langle p_T \rangle / 2$ , consistent with the scale used in the single-jet cross sections when determining the gluon PDFs. With this choice of the scale, all three PDF sets agree with most of the data points within the PDF uncertainty. There appears to be a systematic excess of theory over the data, but its magnitude strongly depends on the assumed factorization scale. For example, it can be much worse if a different scale is taken, such as  $\mu = \langle p_T \rangle$  assumed in Fig.

Figure 6: Ratios of NLO total cross sections obtained using CT10 and CT10W to those using CTEQ6.6M PDFs, in various scattering processes at the Tevatron Run-II and LHC.

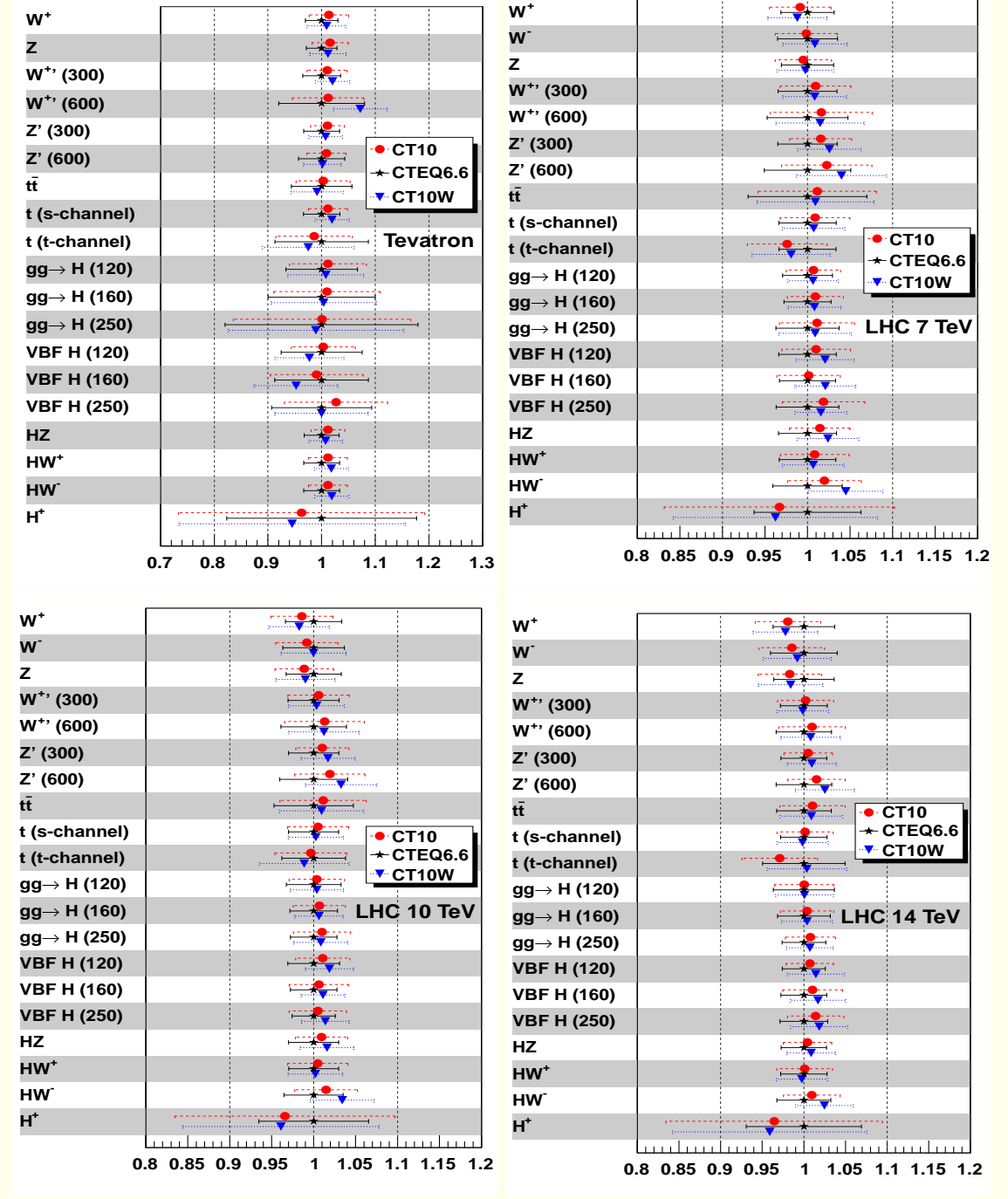
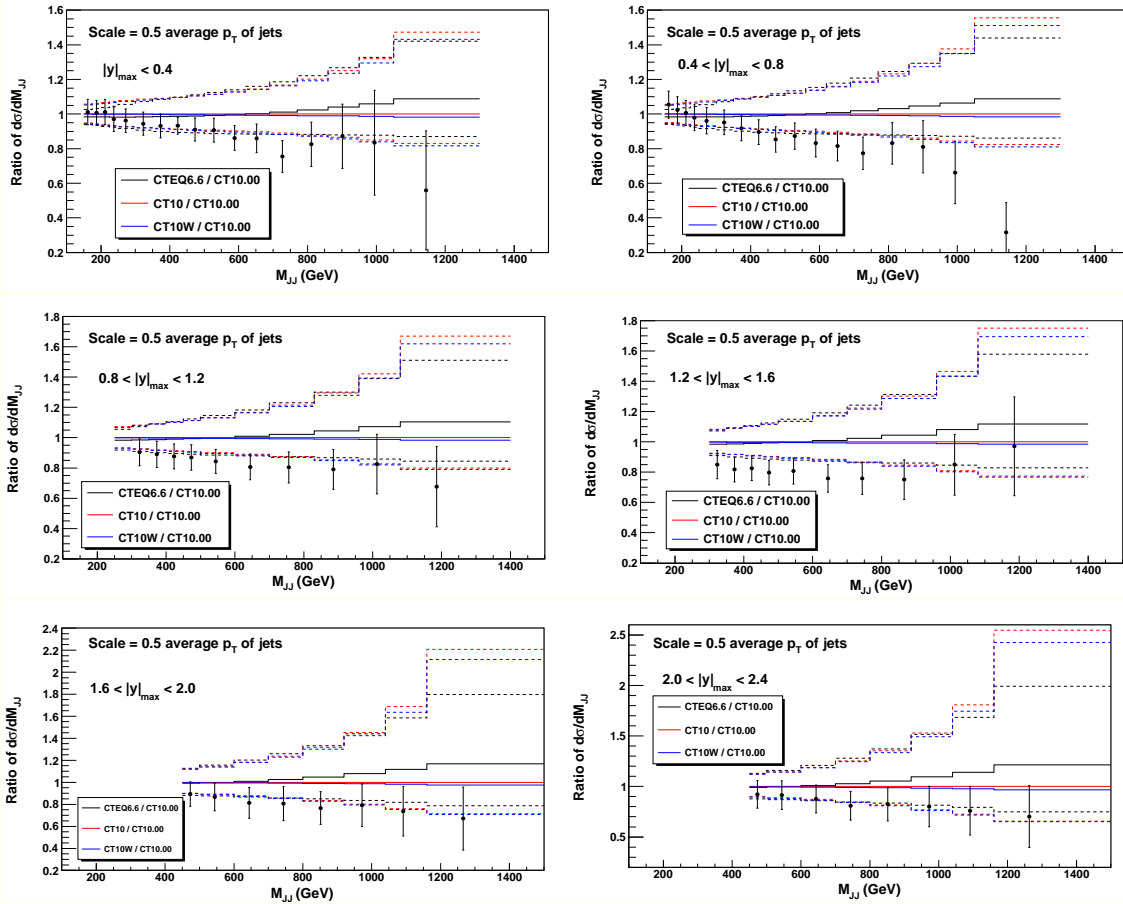


Figure 7: Comparison of  $D\bar{O}$  Run-II data for dijet invariant mass distributions [42] with NLO theoretical predictions and their PDF uncertainties for CTEQ6.6 (black), CT10 (red) and CT10W (blue) PDFs. The cross sections are normalized to theoretical predictions based on the best-fit CT10 set, designated as CT10.00.



2 of the  $D\bar{O}$  paper [42]. We conclude that the CT10 PDFs are reasonably compatible with the  $D\bar{O}$  dijet data within the present theoretical uncertainties, although an overall systematic shift, of order of the systematic shifts observed in the CT09 study of the single-inclusive jet distributions [1], would further improve the agreement, once the full correlated systematic errors of the dijet data become available.

### Uncertainty due to $\alpha_s$ in CTEQ6.6 and CT10 PDF analyses

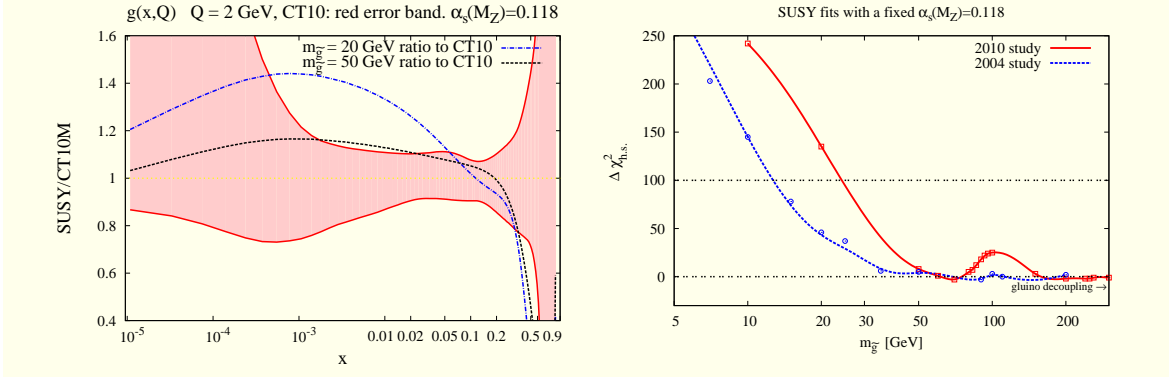
Many calculations for collider processes (*e.g.*, production of  $t\bar{t}$  pairs and Standard Model Higgs bosons) require to evaluate two leading theoretical uncertainties, due to the choice of the PDF parametrization at the initial scale, and the value of the strong coupling constant  $\alpha_s(M_Z)$  assumed in the hard cross sections and the PDFs. These uncertainties can be comparable in size, and their interplay, or correlation, may be important. In Ref. [2], we examine the  $\alpha_s$  dependence of CTEQ6.6 PDFs [7] and show how the PDF- $\alpha_s$  correlations are adequately captured by a simple calculation, without resorting to more elaborate methods proposed in other studies [43].

At the beginning of the PDF fit, one decides which data determine the  $\alpha_s(M_Z)$  value and its uncertainty. CTEQ *best-fit* PDFs and their parametrization uncertainties are usually determined for a constant value of  $\alpha_s(M_Z)$  that is close to its latest world-average central value; *e.g.*,  $\alpha_s(M_Z) = 0.118 \pm 0.002$  assumed in Ref. [2]. This *input* value of  $\alpha_s(M_Z)$  can be viewed as an additional data point that summarizes world constraints on  $\alpha_s$ , mostly determined by precise experiments that are not included in the global fit (notably, LEP event shapes and  $\tau$  and quarkonium decays). In Ref. [2], we explore a more general procedure, in which the world-average data point on  $\alpha_s(M_Z)$  is included in the fit in addition to the usual hadronic scattering data. A theoretical parameter for  $\alpha_s(M_Z)$  is varied in this fit; its *output* value and uncertainty are determined by all input data. We find that the output value of  $\alpha_s(M_Z) = 0.118 \pm 0.0019$  obtained in this way essentially coincides with its input value  $\alpha_s(M_Z) = 0.118 \pm 0.002$ . If the input value is not included, the output uncertainty on  $\alpha_s$  is increased significantly, to  $\alpha_s(M_Z) = 0.118 \pm 0.005$ . This indicates that the hadronic scattering data included in the fit imposes significantly weaker constraints on  $\alpha_s$  than the other experiments contributing to the world-average value.

The Hessian PDF eigenvector sets returned by such floating- $\alpha_s$  fit can be used to estimate the correlation between the PDF parameters and  $\alpha_s(M_Z)$ . However, each of these eigenvector sets is inconveniently associated with its own value of  $\alpha_s(M_Z)$ . Instead, one can apply a simpler procedure, in which all eigenvector sets except two are determined for the best-fit value of  $\alpha_s(M_Z)$ . These eigenvector sets provide the usual PDF uncertainty for a fixed  $\alpha_s(M_Z)$ . Separately, the uncertainty in the PDFs induced by the uncertainty in  $\alpha_s(M_Z)$  is assessed, by producing two alternative PDF fits for the  $\alpha_s(M_Z)$  values at the lower and upper ends of the  $\alpha_s$  uncertainty interval (*i.e.*,  $\alpha_s(M_Z) = 0.116$  and  $0.120$ ). These PDF and  $\alpha_s$  uncertainties are then added in quadrature to obtain the total uncertainty.

This procedure is valid both formally and numerically. It is based on a theorem that is applicable within the quadratic approximation for the log-likelihood function  $\chi^2$  in the vicinity of the best fit. The proof of the theorem, as well as a numerical demonstration of the equivalence of the addition in quadrature to the full estimation of the PDF+ $\alpha_s$  uncertainty based on the Hessian method, are given in Ref. [2]. The series of best-fit PDFs for  $\alpha_s(M_Z)$  values in the interval 0.113-0.123, needed to evaluate the combined PDF+ $\alpha_s$  uncertainty in any application, are made available both for CTEQ6.6 and CT10 PDFs.

Figure 8: Left: Ratio of  $g(x, Q)$  in SUSY fits with a fixed  $\alpha_s(M_Z) = 0.118$  and CT10 fit. Right:  $\Delta\chi^2$  in 2004 and 2010 SUSY fits vs. gluino mass.



### Constraints on new physics from a global PDF analysis

Besides providing the PDFs and their uncertainties, the global QCD analysis can establish bounds on masses of hypothetical particles beyond the standard model (BSM), for example, relatively light color-octet Majorana fermions that contribute to strong interaction processes with the same coupling strength as the gluons. Gluinos of a supersymmetric (SUSY) origin serve as an example of such fermions; but other models can introduce them as well. Constraints on the “gluinos” are often imposed in the context of a specific BSM model for their production and decay, which helps to rule out “gluinos” with masses up to a few hundred GeV. But, if no model-specific assumptions are imposed, much lighter gluinos are allowed: as light as  $\approx 12 - 15$  GeV according to the 2004 global fit based on the CTEQ6 set data [44], or 6-51 GeV according to the NLO/resummation analyses of  $e^+e^-$  hadroproduction at LEP [45, 46, 47]. Note that the limit based on the global fit is not affected by (potentially important) theoretical uncertainties in the LEP analyses, associated with nonperturbative and matching effects in the resummation techniques that they employ.

In Ref. [48], we improve the earlier limits [44] on relatively light gluinos based on an extended CT10 fit with added gluino scattering contributions. In this study, an independent PDF describing gluinos, and one-loop splitting functions describing interactions of gluinos with quarks and gluons, are introduced in the DGLAP equation. Two-loop gluino contributions are included in the renormalization group equation for the running of  $\alpha_s$ . Cross sections for single-inclusive jet production are modified to include hard matrix elements for  $2 \rightarrow 2$  processes involving gluinos, with full dependence on the gluino mass evaluated in the general-mass factorization scheme. These modifications capture the essential dependence on gluinos in inclusive processes studied in the CT10 fits. Generally, the gluino contributions to inclusive observables are small, so that they can be evaluated at the one-loop level to achieve the same accuracy as the SM contributions evaluated at two loops. Squarks and other BSM particles are assumed to be heavier than a few hundred GeV and not included.

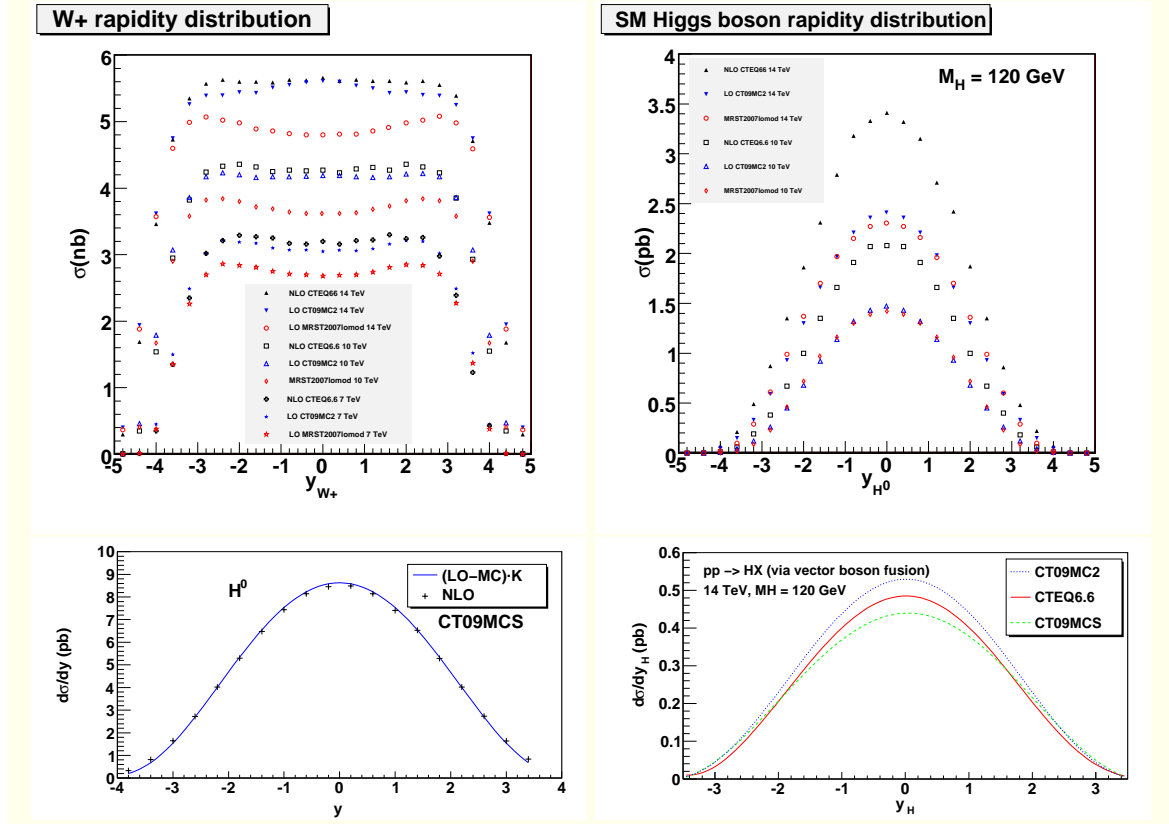
Constraints on the gluino mass  $m_{\tilde{g}}$  depend strongly on the value of  $\alpha_s(M_Z)$  [44]. To reproduce the existing limits on  $\alpha_s(Q)$ , we introduce two data points at  $Q = 5$  GeV and  $M_Z$ , representing a combination of measurements at low  $Q$  and  $Q \approx M_Z$ , respectively. The low- $Q$  bound on  $\alpha_s$  has been obtained by combining measurements of  $\alpha_s(M_Z)$  in  $\tau$  and quarkonium decays. These low- $Q$

measurements are not affected by gluinos heavier than 10 GeV. Gluino contributions to the high- $Q$  data point are of the same order as the experimental uncertainties.

With the  $\alpha_s$  data and latest hadronic data included, the 2010 SUSY PDF fits reduce the allowed range of gluino masses, as compared to the 2004 fits [44]. For example, Fig. 8 illustrates SUSY fits with a constant QCD coupling strength,  $\alpha_s(M_Z) = 0.118$ , for gluino masses  $m_{\tilde{g}}$  shown in the figure. The left subfigure compares the gluon PDF obtained in SUSY fits with  $m_{\tilde{g}} = 20$  and 50 GeV (solid lines) to the CT10 error band (corresponding to  $m_{\tilde{g}} = \infty$ ). It is clear that too light gluinos distort the shape of the CT10 gluon PDF to an unacceptable level. The right subfigure shows the differences  $\Delta\chi^2 = \chi^2(\alpha_s, m_{\tilde{g}}) - \chi^2_{CT10}$ . One can see that  $\Delta\chi^2 > 100$  for  $m_{\tilde{g}} < 25$  GeV, suggesting that gluinos lighter than 25 GeV are excluded at about 90% C.L., for  $\alpha_s(M_Z) = 0.118$ . This improves the 2004 constraint [44],  $m_{\tilde{g}} > 12$  GeV for  $\alpha_s(M_Z) = 0.118$ , by a factor of two. Similarly, the 2004 limit on  $m_{\tilde{g}}$  for a free  $\alpha_s$ , which allowed  $m_{\tilde{g}} = 1$  GeV for  $\alpha_s(M_Z) = 0.135$ , is increased to  $m_{\tilde{g}} > 13$  GeV for any  $\alpha_s$  in the 2010 fit.

Gluinos with mass about 50 GeV remain allowed both by the global fits and LEP data analysis. Such light gluinos may alter cross sections for jet production and other LHC processes [48]. We provide tables of PDFs with contributions of gluinos in this mass range to explore phenomenological implications.

Figure 9: Rapidity distributions of  $W^+$  and Higgs bosons computed with LO-MC and NLO PDF's.



## PDFs for leading-order showering programs

Monte Carlo event generators, especially, the most mature leading-order generators, play a critical role in all stages of modern particle physics. Neither conventional LO PDFs, nor NLO PDFs produce satisfactory results when implemented in the showering programs. In Ref. [4], we modified the usual leading-order global analysis to find optimized PDFs for leading-order Monte-Carlo (LO-MC) simulations at the LHC. Besides the usual constraints from the existing hard-scattering experimental data, the joint input of this analysis incorporates pseudodata points for cross sections of  $W$ ,  $Z$ ,  $t\bar{t}$ , SM Higgs, and  $gg \rightarrow bb'$  production at the LHC, as *predicted* by NLO QCD theory. The PDFs resulting from this analysis are not strictly at the leading order: they include some information about key LHC processes evaluated at NLO. Event generators, including "LO event generators", have some elements of higher-order contributions and, in this sense, are not at the stated order in the QCD coupling. We can use their flexibility to find the LO-MC PDFs that better reproduce the benchmark NLO cross sections, when combined with LO matrix elements in a fixed-order calculation or a LO event generator.

To examine the available possibilities, we provide three representative LO-MC PDF sets, designated as CT09MCS, CT09MC1, and CT09MC2. These PDFs realize different strategies for bringing the LO predictions closer to NLO. Their differences stem from varying assumptions about the running of  $\alpha_s$  (evaluated at one or two loops), factorization scales in the LHC pseudodata cross sections (fixed or fitted), and the momentum sum rule imposed on the PDFs (exact or relaxed by 10-15% [49]). An example of the LO-MC PDFs in action is shown in Fig.9, which compares cross sections for  $W^+$  boson and Standard Model Higgs boson rapidity distributions at the LHC, obtained with LO matrix elements and CT09MC2 and MRST2007lomod PDFs [49], and at NLO with CTEQ6.6. In the  $W^+$  production case (upper left subfigure), the CT09MC2 calculation closely reproduces both the normalization and shape of the NLO cross section at all three LHC energies, while the MRST2007lomod prediction differs from NLO in normalization at  $\sqrt{s} = 7$  TeV, and both in normalization and shape at 10 and 14 TeV. For Higgs production (upper right subfigure), both CT09MC2 and MRST2007lomod predictions provide almost identical distributions, which are smaller than the NLO prediction by a nearly constant normalization factor. This difference with NLO reflects especially large virtual corrections present in Higgs production cross sections, which cannot be completely compensated by an increase in the LO gluon density. However, since the average normalization factors  $K$  for each pseudodata process are also known from the fit (and published in our paper), end users can multiply the LO-MC cross sections for Higgs production and other pseudodata processes by these K-factors to better approximate the NLO cross sections (cf. the lower left subfigure). If an LHC process is not included as the pseudodata, comparison of LO predictions based on several LO-MC sets may still provide a reasonable estimate of the NLO cross section, as illustrated by the cross section for SM Higgs boson production via vector boson fusion in the lower right subfigure.

In summary, the CT10 and CT10W sets are based on the most up-to-date information about the PDFs available from global hadronic experiments. There are 26 free parameters in both new PDF sets; thus, there are 26 eigenvector directions and a total of 52 error PDFs for both CT10 and CT10W. The CT10 and CT10W PDF error sets, along with the accompanying  $\alpha_s$  error sets, allow for a complete calculation of the combined PDF+ $\alpha_s$  uncertainties for any observable.

## Acknowledgments

This work was supported in part by the U.S. Department of Energy under Grants DE-AC02-06CH11357, DE-FG02-04ER41299, and DE-SC0003870; by the U.S. National Science Foundation

under grant PHY-0855561; by the National Science Council of Taiwan under grants NSC-98-2112-M-133-002-MY3 and NSC-99-2918-I-133-001; and by Lightner-Sams Foundation.

## References

- [1] J. Pumplin et al., Phys. Rev. D80 (2009) 014019.
- [2] H. L. Lai, J. Huston, Z. Li, P. Nadolsky, J. Pumplin, D. Stump and C.-P. Yuan, Phys. Rev. D **82**, 054021 (2010).
- [3] H. L. Lai, M. Guzzi, J. Huston, Z. Li, P. M. Nadolsky, J. Pumplin and C.-P. Yuan, Phys. Rev. D **82**, 074024 (2010).
- [4] H.L. Lai et al., JHEP 04 (2010) 035.
- [5] A.D. Martin et al., Eur. Phys. J. C63 (2009) 189.
- [6] R.D. Ball et al., Nucl. Phys. B838 (2010) 136, 1002.4407.
- [7] P.M. Nadolsky et al., Phys. Rev. D78 (2008) 013004.
- [8] The HERA and ZEUS Collaborations, F.D. Aaron et al., JHEP 01 (2010) 109.
- [9] The CDF Collaboration, D. Acosta et al., Phys. Rev. D71 (2005) 051104.
- [10] The DØ Collaboration, V.M. Abazov et al., Phys. Rev. Lett. 101 (2008) 211801.
- [11] The DØ Collaboration, V.M. Abazov et al., Phys. Rev. D77 (2008) 011106.
- [12] T. A. Aaltonen *et al.* [CDF Collaboration], Phys. Lett. B **692**, 232 (2010).
- [13] The DØ Collaboration, V.M. Abazov et al., Phys. Rev. D76 (2007) 012003.
- [14] The CDF Collaboration, T. Aaltonen et al., Phys. Rev. D78 (2008) 052006.
- [15] The DØ Collaboration, V.M. Abazov et al., Phys. Rev. Lett. 101 (2008) 062001.
- [16] <http://projects.hepforge.org/lhapdf/>.
- [17] The CTEQ-TEA Collaboration, <http://hep.pa.msu.edu/cteq/public/ct10.html>.
- [18] P.M. Nadolsky and Z. Sullivan, (2001), hep-ph/0110378.
- [19] F. Caola, S. Forte and J. Rojo, Phys. Lett. B686 (2010) 127.
- [20] F. Caola, S. Forte and J. Rojo, (2010), arXiv:1007.5405.
- [21] E.L. Berger et al., Phys. Rev. D40 (1989) 83.
- [22] S. Catani, G. Ferrera and M. Grazzini, JHEP **1005**, 006 (2010).
- [23] A.D. Martin, R.G. Roberts and W.J. Stirling, Mod. Phys. Lett. A4 (1989) 1135.
- [24] H.L. Lai et al., Phys. Rev. D51 (1995) 4763.

- [25] C. Balazs, J. w. Qiu and C. P. Yuan, Phys. Lett. B **355**, 548 (1995).
- [26] C. Balazs and C. P. Yuan, Phys. Rev. D **56**, 5558 (1997).
- [27] F. Landry, R. Brock, P. M. Nadolsky and C. P. Yuan, Phys. Rev. D **67**, 073016 (2003).
- [28] P. B. Arnold, R. K. Ellis and M. H. Reno, Phys. Rev. D **40**, 912 (1989).
- [29] P. B. Arnold and M. H. Reno, Nucl. Phys. B **319**, 37 (1989) [Erratum-ibid. B **330**, 284 (1990)].
- [30] W. T. Giele, E. W. N. Glover and D. A. Kosower, Nucl. Phys. B **403**, 633 (1993).
- [31] J. M. Campbell and R. K. Ellis, Phys. Rev. D **65**, 113007 (2002).
- [32] K. Melnikov and F. Petriello, Phys. Rev. D **74**, 114017 (2006)
- [33] R. Gavin, Y. Li, F. Petriello and S. Quackenbush, arXiv:1011.3540 [hep-ph].
- [34] S. Catani, L. Cieri, G. Ferrera, D. de Florian and M. Grazzini, Phys. Rev. Lett. **103**, 082001 (2009).
- [35] P. M. Nadolsky, 2008, unpublished.
- [36] R. Ball *et al.* [The NNPDF Collaboration], arXiv:1012.0836 [hep-ph].
- [37] The CDF Collaboration, F. Abe *et al.*, Phys. Rev. Lett. **74** (1995) 850.
- [38] The New Muon Collaboration, P. Amaudruz *et al.*, Phys. Lett. B **295** (1992) 159.
- [39] The BCDMS Collaboration, A.C. Benvenuti *et al.*, Phys. Lett. B **223** (1989) 485.
- [40] The BCDMS Collaboration, A.C. Benvenuti *et al.*, Phys. Lett. B **237** (1990) 592.
- [41] E. L. Berger, J. Qiu and R. A. Rodriguez-Pedraza, Phys. Rev. D **76**, 074006 (2007).
- [42] The DØ Collaboration, V.M. Abazov *et al.*, (2010), arXiv:1002.4594.
- [43] A.D. Martin *et al.*, Eur. Phys. J. C **64** (2009) 653.
- [44] E.L. Berger *et al.*, Phys. Rev. D **71** (2005) 014007.
- [45] P. Janot, Phys. Lett. B **564** (2003) 183.
- [46] ALEPH Collaboration, A. Heister *et al.*, Eur. Phys. J. C **31** (2003) 327.
- [47] D.E. Kaplan and M.D. Schwartz, (2008), arXiv:0804.2477.
- [48] E. L. Berger, M. Guzzi, H.-L. Lai, P. M. Nadolsky, F. I. Olness, Phys. Rev. D **82**, 114023 (2010).
- [49] A. Sherstnev and R.S. Thorne, Eur. Phys. J. C **55** (2008) 553, 0711.2473.